Chapter 4

DCE-MRI: acquisition and analysis techniques

Paul S. Tofts and Geoff J. M. Parker

Key points

- DCE-MRI uses dynamic T_1-weighted imaging after bolus administration of Gd-based contrast agent to estimate parameters which describe blood flow and tissue permeability.
- Accurate measurements require an arterial input function (AIF) to be sampled, pre-contrast tissue T_1 (T_{10}) to be measured, and the flip angle of the imaging sequence to be precisely set.
- Modeling of DCE-MRI data usually yields the transfer constant (K^{trans}), volume of the extravascular extracellular space (v_e), and the rate constant k_{ep} ($K^{trans} = v_e \times k_{ep}$).
- More sophisticated models also estimate other parameters such as the vascular plasma volume (v_p) and flow (F).
- Measurements may either be "flow-limited" ($K^{trans} = F(1 - Hct)$, where Hct is the blood hematocrit), or "permeability-limited" ($K^{trans} = PS$, the permeability surface area product), depending on the relative magnitudes of F and PS.
- When flow (F) and permeability (PS) are comparable, more sophisticated modeling can be used; however, care should be taken not to over-interpret the data (i.e., not to fit too many model parameters if data are limited or noisy).
- The MRI protocol to be used, and optimal temporal resolution and length of sampling, depends on the organ system to be studied; for tumors, scan time should be at least 5–10 min; if the "plateau" phase of enhancement is not reached, v_e may not be accurately estimated.
- In evaluating anti-angiogenic cancer therapies, the consensus is that K^{trans} should be the primary outcome variable from DCE-MRI experiments.

Introduction

There are increasing opportunities to use dynamic contrast-enhanced (DCE) T_1-weighted imaging to characterize tumor and other pathological biology and treatment response, using modern fast sequences that can provide good temporal and spatial resolution combined with good organ coverage [1]. Quantification in MRI is recognized as an important approach to characterize tissue biology. This chapter provides an introduction to the physical concepts of mathematical modeling, image acquisition, and image analysis needed to measure aspects of tissue biology using DCE imaging, in a way that should be accessible for a research-minded clinician.

Quantification in MRI represents a paradigm shift, a new way of thinking about imaging [2]. In qualitative studies, the scanner is a highly sophisticated camera, collecting images that are viewed by an experienced radiologist. In quantitative studies, the scanner is used as a sophisticated measuring device, a scientific instrument able to measure many properties of each tissue voxel (e.g., T_1, T_2, diffusion tensor, magnetization transfer, metabolite concentration, K^{trans}). An everyday example of quantification would be the bathroom scales, used to measure our weight. We expect that the machine output shown on the dial, in kg, will be accurate (i.e., close to the true value), reproducible (i.e., if we make repeated measurements over a short time they will not vary), reliable (the scales always work), and biologically relevant (the quantity of weight does indeed relate to our health). An example of a clinical measurement

Clinical Perfusion MRI: Techniques and Applications, ed. Peter B. Barker, Xavier Golay, and Greg Zaharchuk. Published by Cambridge University Press.

would be a blood test; we expect it to work reliably every time. This is the aspiration for quantitative MRI: that it should deliver a high-quality measurement that relates only to the patient biology (and not the state of the scanner at the time of measurement).

A popular measurement derived from DCE-MRI is the transfer constant, K^{trans} (see below, or refer to Chapter 1), which characterizes the diffusive transport of low-molecular weight gadolinium (Gd) chelates across the capillary endothelium [3]. K^{trans} has been widely used in imaging studies to characterize tumor biology and treatment response. The fractional volume v_e of the extravascular extracellular space (EES; i.e., the interstitial space), can also be measured. A consensus recommendation [4] proposed that in assessing anti-angiogenic and anti-vascular therapies in cancer, K^{trans} should be a primary readout (endpoint). Secondary endpoints should include v_e, the rate constant k_{ep} $\left(k_{ep} = K^{trans}/v_e\right)$, and the plasma volume v_p (if available from the modeling process). The traditional clinical evaluation of tumor treatment uses the RECIST criteria, based on tumor diameter; however, effective non-cytotoxic therapies do not necessarily induce rapid tumor shrinkage, and markers such as K^{trans} and v_e may often be more sensitive markers of the effect a drug has on a tumor. There are also applications of DCE-MRI in tissues other than tumors, e.g., renal and myocardial function, and assessment of inflammation in the lung and joints; this chapter focuses on DCE-MRI methods and is illustrated with applications in tumors and other pathologies, with one example of normal renal function.

Although K^{trans} is not a direct measurement of perfusion, it is often sensitive to perfusion (see below, Eqs (4.7), and (4.8). Explicit estimation of perfusion (F) is also possible with appropriate modeling techniques (see below), although often their use demands advanced rapid imaging methods, which are not currently widely available.

Modeling

The signal data modeling process for DCE-MRI can be considered as having two components [5]. First, the Gd contrast agent concentration has to be found from the MRI signal enhancement. Second, given the Gd concentration as a function of time, pharmacokinetic analysis can then be undertaken to model how the contrast agent distributes in the body, and how this depends on physiological parameters. This is independent of the imaging conditions (MRI field strength, etc.), and in principle also independent of imaging modality (for example whether computed tomography (CT) or MRI [6, 7]). Given the characteristics of the modeling, this then guides the choice of imaging sequence (see the section on image acquisition)

MRI modeling: finding Gd concentration from MRI signal

The MRI Gd concentration model has in turn two components. First, T_1 is reduced from its native value T_{10} by the presence of a concentration c of Gd:

$$\frac{1}{T_1} = \frac{1}{T_{10}} + r_1 c \tag{4.1}$$

Often it is more convenient to use the relaxation rate $R_1 = 1/T_1$:

$$R_1 = R_{10} + r_1 c \tag{4.2}$$

The longitudinal relaxivity r_1, (i.e., the constant of proportionality between Gd concentration and increase in relaxation rate $R_1 = 1/T_1$) is specific to a contrast agent and varies with field strength. For example, the relaxivity of Gd-DTPA (Magnevist) is usually assumed to be equal to the in vitro value of $4.5\,s^{-1}\,mM^{-1}$ (measured in aqueous phantoms at 1.5 T [8]), although it may be different in vivo [9, 10]. Note that in order to calculate c, the native tissue (or lesion) T_1 (i.e., the value before injection of contrast agent, T_{10}) must also be known. Note that to apply Eqs. (4.1) and (4.2) to total tissue Gd concentration one has to implicitly assume fast water exchange between tissue compartments, i.e., that all the Gd in a voxel is available to relax all of the water, whether it is residing in the blood pool, the extravascular extracellular (interstitial) space or the intracellular space.

Second, the way in which the T_1 reduction increases the signal is modeled; this is specific to each sequence type. The most common sequence used for this purpose is the simple spoiled gradient echo ("FLASH" or "GRE"), on account of its ability to combine good volume coverage, acceptable spatial resolution, acceptable precision and accuracy, and acceptable acquisition speed. The signal S from a spoiled gradient echo sequence is:

$$S = S_0 \frac{\left(1 - e^{-TR/T_1}\right)\sin\,\theta}{1 - e^{-TR/T_1}\cos\,\theta} \tag{4.3}$$

where S_0 is the relaxed signal (i.e., equal to S when $TR \gg T_1$, $\theta = 90°$), and θ is the flip angle (FA). Note that this equation assumes echo time (TE) $<< T_2^*$. S_0

can be found from the measured pre-Gd signal (before injection of contrast agent).

The sequence must be truly "spoiled" (i.e., there is no build up of steady-state transverse magnetization) and the FA used must be known (if necessary by employing a B_1 mapping method). Provided that the three parameters (r_1, T_{10}, and FA) are known, then there is a clear relationship between signal and the change in T_1 (i.e., the Gd concentration) (Eq (4.3)).

To find the arterial plasma concentration, which will be required if pharmacokinetic modeling is to be performed, one needs first to find the blood concentration $c_b(t)$ from the blood signal, using Eqs. (4.1) and (4.3). Blood T_{10} is about 1.4 s at 1.5 T [11]. Since the contrast agent is only present in the extracellular space, the plasma concentration $c_p(t)$ is higher, by a factor related to the hematocrit Hct, e.g., a factor of 1.7 for Hct = 41%[12]. Note that Hct can vary considerably between patients and over time in patients undergoing treatment [13]:

$$c_p = \frac{c_b}{1 - Hct} \tag{4.4}$$

Some studies attempt to find Gd concentration from signal by using a phantom calibration curve; however, these approaches are usually flawed, since the signal is also proportional to proton density (which is greater in an aqueous solution than in tissue), and the FA may be different when imaging the phantom (caused for example by different coil loading and/or B_1 inhomogeneity).

Pharmacokinetic modeling: from Gd concentration to physiology

"Tofts' model": K^{trans}, v_e, and k_{ep}

Most modeling uses the concept of a compartment; this is like a bucket: the Gd tracer inside is dissolved in water and at the same concentration everywhere, and the flow into or out of the bucket is small enough to allow the contents to remain well mixed.

The simplest compartmental model has one tissue compartment in addition to a vascular compartment. This is known as the "Tofts' model" [5] (mathematically equivalent to that proposed by Kety [14] in a non-MRI context), and may be used to measure K^{trans} and v_e (see Figure 4.1). The bolus injection of Gd gives a time-varying blood plasma concentration $c_p(t)$, which can be measured in each subject, or if not available estimated from a population average [15–17]. Since the commonly used contrast agents are small ($<\approx 1000$ Daltons) then the leakage across the endothelium from the capillaries into the EES is generally accepted to be diffusive, passive, and hence reversible; it is therefore proportional to the difference between the concentrations in the plasma and in the EES (c_p and c_e respectively).

$$v_e \frac{dc_e(t)}{dt} = K^{trans}\left(c_p(t) - c_e(t)\right) \tag{4.5}$$

K^{trans} is the constant of proportionality, and $v_e c_e$ is the amount of Gd in the EES. Formally, K^{trans} is the volume transfer constant between the blood plasma and the EES [3]. Clearance from the blood is usually renal, although biliary clearance is also possible, depending on the contrast agent.

The solution to this equation is a convolution of c_p with the impulse response function $K^{trans}\exp(-k_{ep}t)$ [18]; when the intra vascular Gd is taken into account, the total "tissue" concentration is:

$$c_t(t) = v_p c_p(t) + K^{trans}\int_0^t c_p(\tau)e^{-k_{ep}(t-\tau)}d\tau \tag{4.6}$$

Thus the total Gd concentration in a voxel or region of interest(ROI) (Eq. 4.6) is the sum of the EES

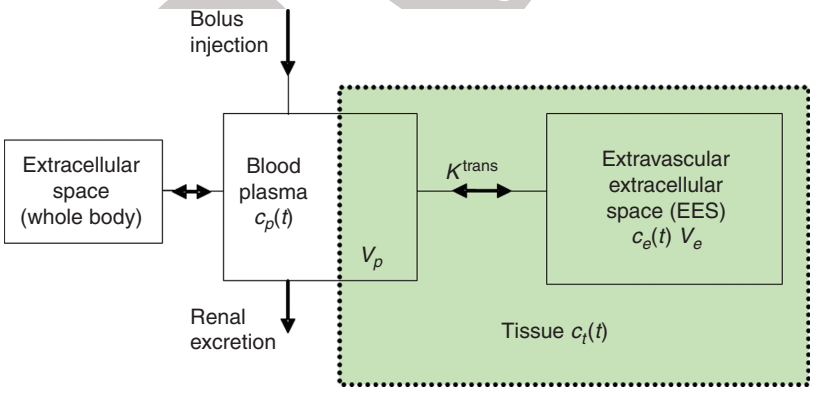

Figure 4.1 A simple compartmental model used for DCE-MRI data analysis.

contribution (which usually dominates, since $v_e \approx 10$–60%) and the intravascular contribution (the "v_p term"), which is often small and in some cases ignored ($v_p \approx 1$–10%) [18]. The original "Tofts' model" [5] had no v_p term. The "extended Tofts' model" [18] refers to Eq. (4.6), with the v_p term present.

This model was able to explain signal enhancement in multiple sclerosis lesions [5] (Figure 4.2), and gave values of K^{trans} and v_e consistent with the known biology of acute and chronic lesions.

The differences in enhancement curve shape, and the time of peak enhancement, both apparent in Figure 4.2, are important. A model simulation [5] using typical K^{trans} values for tumors and neglecting the influence of any intravascular Gd (i.e., $v_p = 0$), shows that the initial slope depends on K^{trans} (Figure 4.3a), and is independent of v_e (Figure 4.3b). The final peak value depends on v_e, and larger v_e tumors take longer to reach their peak (Figure 4.3b). The shape of the curve is determined by k_{ep}, and if K^{trans} is increased whilst keeping k_{ep} fixed, the curve increases in amplitude but retains the same shape (Figure 4.3c) as is expected from Eq. (4.6).

In the original formulation of the model (applied to multiple sclerosis), trans-endothelial leakage was low enough that there would not be significant local depletion of Gd concentration in the capillary. Perfusion F was sufficient to maintain the capillary concentration at the arterial value. In this case, K^{trans} is just the permeability surface area product (PS), and DCE could reasonably be called "permeability imaging." This "permeability-limited" case is defined by $F \gg PS$:

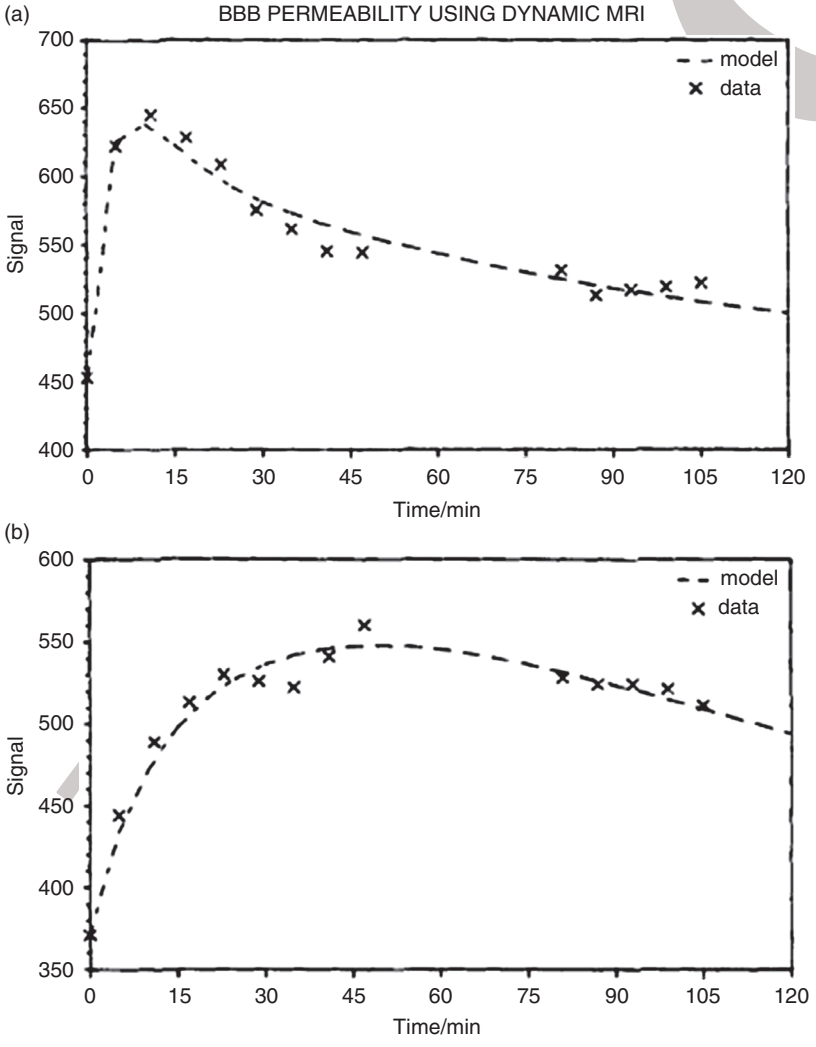

Figure 4.2 Use of DCE-MRI to measure capillary leakage in a patient with multiple sclerosis [5]. The upper plot shows enhancement in an acute multiple sclerosis lesion. The signal peaks at about 12 min, model fitting gave $K^{trans} = 0.050\ min^{-1}$, $v_e = 21\%$. The lower plot shows a chronic lesion with a less permeable blood-brain barrier ($K^{trans} = 0.013\ min^{-1}$), and an enlarged EES ($v_e = 49\%$), with signal peaking later (at about 50 min). These data were collected in 1989 using a multi-slice spin echo sequence; note the poor temporal resolution by modern standards, and the missing data when the patients took a break. BBB, blood–brain barier.

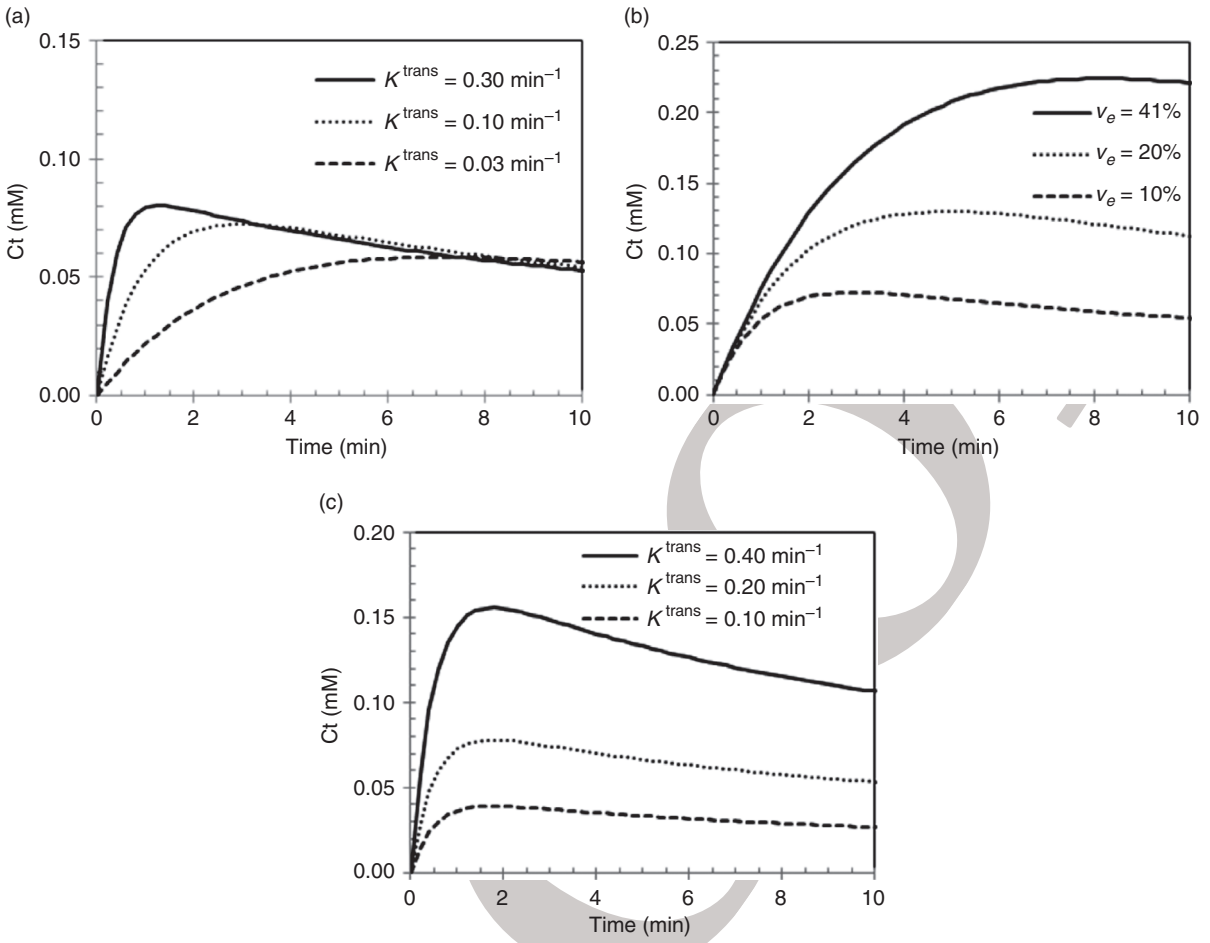

Figure 4.3 Simulations of tissue concentration after bolus injection of 0.1 mmol/kg of Gd, for a range of K^{trans} and v_e values, ignoring any intravascular contribution. (a) increasing K^{trans}, with fixed $v_e = 10\%$ (b) increasing v_e, with fixed $K^{trans} = 0.1\ min^{-1}$ (c) constant $k_{ep} = 2\ min^{-1}$, increasing K^{trans}.

$$K^{trans} = PS(F \gg PS) \quad (4.7)$$

In tumors, the endothelium can be much more leaky, there may be local depletion from the vasculature, and K^{trans} will represent a combination of permeability and perfusion [3]. In the limiting case of very high permeability, then K^{trans} will equal the plasma perfusion $\left(F_p = F(1 - Hct)\right)$, and DCE could reasonably be called "perfusion imaging." This is the "flow-limited case", defined by F≪PS.

$$K^{trans} = F(1 - Hct) \quad (F \ll PS) \quad (4.8)$$

The significance of K^{trans} under various values of F, PS, and v_p is explored in the reviews by Sourbron and Buckley [19, 20].

Perfusion is here used to mean the supply of blood to tissue (units: ml blood/min/100 ml tissue), and we have assumed that all blood passing into a volume of tissue is available for capillary exchange. Perfusion is the preferred term here [4]. It is sometimes called "blood flow," as used in some other chapters throughout this book. Note that in that case, the term may be ambiguous, as "flow" may also mean blood flow velocity (in m/s).

Blood perfusion F can be estimated from K^{trans} (Eq. 4.7) in the PS-limited case, provided Hct is known. However small-vessel hematocrit Hct^{small} can be considerably lower than in large vessels (where the AIF is measured). This is related to the Fahraeus effect; in small vessels the red blood cells are comparable in size to the vessel diameter, and travel faster than plasma [21]. Values for Hct^{small} are hard to measure; values of 24% (dog heart) [22], 31% (human brain) [23], 25% [24], and 8–20% [21] have been

reported. The renal vasa recta (10–20 μm in diameter) have a reduced hematocrit of 40–50% compared with a large vessel [25]. Thus estimates of F are vulnerable to large uncertainties in Hct [26, 27].

Since the contrast agent is transported in the plasma, plasma perfusion F_p is more reliably measured than blood perfusion F. Thus there is a move to using F_p rather than F as the relevant biomarker in DCE-MRI [20, 26, 27].

The modeling of the capillary vasculature shown in Figure 4.1 is naive, and not surprisingly at high temporal resolution it fails. Modern sequences can sometimes provide a temporal resolution of ~1 s (depending on the organ, resolution, and coverage required), and in these cases the initial rise in signal gives information about perfusion, as Gd arrives in the capillary bed over a few seconds. More sophisticated models are then able to extract pure perfusion information [28, 29], and potentially pure permeability information as well. In DCE kidney imaging, the perfusion peak in tissue is clearly delayed (by about 4 s) with respect to the arterial peak (see Figure 4.4).

Other pharmacokinetic models

Other models have been proposed that aim to extract estimates of perfusion F from the DCE-MRI time series. These fall into three broad categories:

Bolus passage perfusion estimates

In some organs, notably the lung [30, 31] and the heart [32], T_1-weighted DCE-MRI measurements have been modeled in a similar fashion to bolus passage dynamic susceptibility contrast (DSC) measurements that historically have found application in the brain. The reason for this is partly physiological – these organs have a large blood volume – and partly pragmatic – the DCE-MRI measurements typically require breath-hold in both the lung and heart and therefore it is convenient to measure only the first passage. By restricting analysis to this early phase of the contrast agent delivery to the tissue it is often possible to ignore the effects of contrast agent leakage or to assume that any leakage that does occur is unidirectional (i.e., from the blood to the EES only, as there is not time for measureable leakage in the opposite direction). This allows methods such as the indicator dilution theorem to be applied [31], whilst not precluding full compartmental analysis if deemed necessary [32, 33]

Two compartment exchange model (2CXM)

As discussed above, the model described in Eq. 4.6 allows the parameter K^{trans} to be interpreted either as the permeability surface area product (PS) or as perfusion (F), depending on the relative magnitudes of PS and F. The 2CXM addresses this ambiguity by explicitly modeling a perfusion component influencing the signal in the blood pool [29, 34, 35]

$$v_p \frac{dc_p(t)}{dt} = F(c_a - c_p) - K_{PS}(c_p - c_e) \tag{4.10}$$

and

$$v_e \frac{dc_e(t)}{dt} = K_{PS}(c_p - c_e) \tag{4.11}$$

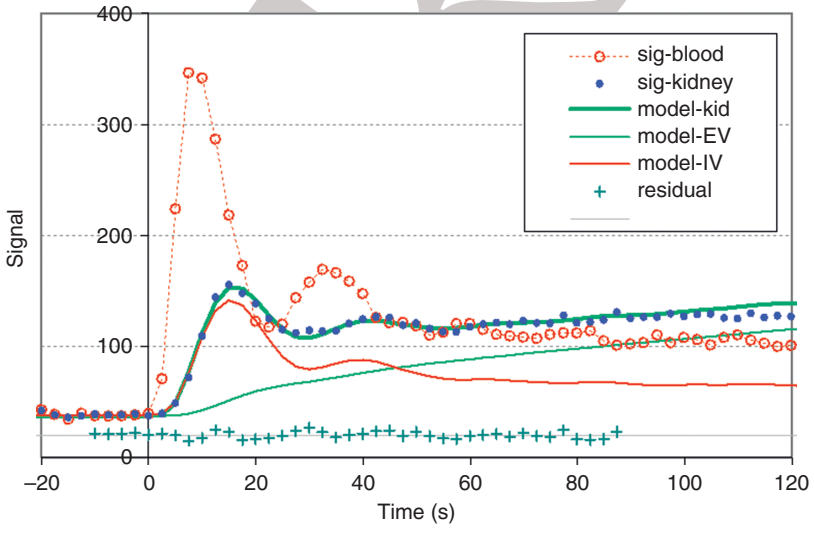

Figure 4.4 Model analysis of renal enhancement. The kidney signal (sig-kidney) is clearly delayed (by about two time points) from the blood signal (sig-blood). The model fit (model-kid) shows separately the extravascular filtered Gd (model-EV, from which glomerular fitteration rate [GFR] is found) and the intravascular Gd (model-IV, from which blood volume and perfusion are estimated).

where c_a is the AIF (i.e., the Gd concentration in a supplying artery), c_p is the tissue blood plasma concentration, and K_{PS} is the equivalent of K^{trans} (a transfer constant between the blood plasma space and the EES) but now the F versus PS ambiguity has been removed. While this is clearly an attractive benefit of this approach, the fact that an additional model parameter is extracted from the data imposes additional data quality requirements, and a careful statistical assessment should be performed to ensure that use of the more complex model is justified [33] [36].

Tissue homogeneity model

The tissue homogeneity model explicitly models the gradient in contrast agent concentration along a capillary induced due to the progressive leakage of contrast agent from the start to the end of the capillary bed [28, 37, 38]. It no longer conforms to the concept of a compartmental model with well-mixed compartments and is therefore sometimes referred to as a distributed parameter model. The modeling of the gradient in concentration along the capillary necessitates the incorporation of a transit time along the capillary, which in turn provides information on blood flow. The model has been simplified as the *adiabatic approximation to the tissue homogeneity model* (*AATH*) and applied to extract blood flow information using DCE-MRI in a range of tissues [28, 33]. As with the 2CXM, fitting of the AATH model requires additional parameter definition, with the subsequent need for careful assessment of the quality of the support for the model provided by the DCE-MRI data.

Heuristic methods

Other, simpler, methods are also used in DCE analysis. These include extraction of parameters such as inital slope, time to peak, and maximum enhancement. If the data acquisition is correctly configured, then these do not require knowledge of parameters that characterize the imaging sequence (e.g., FA) and the tissue (e.g., T_{10}) and are very simple to implement (there is no fitting process). However, errors in FA and variations in tissue native T_1 can have a substantial impact on image contrast and this can also affect heuristic parameterizations (an extreme example is if the FA is so small as to remove all useful T_1 contrast and no enhancement is observed). These parameterizations also usually have increased variability within and between subjects and between MR scanners, are dose-dependent, and the calculated tissue parameters may have no clear relationship to the underlying biological tissue characteristics.

Image acquisition

Imaging protocol

In DCE imaging, repeated T_1-weighted images are collected for several frames before Gd is injected, and then for several minutes afterwards. This is often preceded by a T_1 measurement. A good bolus injection can be achieved by using a power injector, with a saline flush after the Gd. The receiver and transmitter gains must be controlled for the whole series of DCE images.

Quality assurance [2, 39] can be used to ensure the scanner is stable for the DCE acquisition period. A phantom at constant temperature can be repeatedly imaged (this can also be used to check T_1 accuracy), or else one or more healthy volunteers can be repeatedly scanned (without Gd).

The sequence parameters will involve compromise between coverage, temporal resolution, and spatial resolution. Newer scanners have faster gradients (allowing shorter repetition times [TRs]), and multi-array receive coils give higher signal-to-noises ratio at short TRs. The optimal sequence will depend on the organ being measured; often frame times of 2–20 s can be achieved when using spoiled gradient echo methods. Three-dimensional (volume) sequences are preferred, since they have better FA accuracy than 2D (slice-selective) sequences and provide good volume coverage. Body coil transmission gives better FA accuracy than combined transmit/receive coils, but B_1 mapping may still be desirable, particularly in abdominal studies and at higher field strengths (3 T and above). In the abdomen, a coronal-sagittal oblique slice orientation (instead of transverse) can have two advantages: the aorta can be sampled along its length, reducing wash-in effects, and breathing movement is mostly in-plane and therefore more easily corrected. However, coronal-sagittal oblique methods are not always able to sample simultaneously the aorta and the organ or tumor of interest, so transverse acquisitions are more generally applicable, particularly if an effective motion correction strategy is employed [40].

The blood signal curve may be measured, in order to provide an AIF for the modeling. In this case a temporal resolution of ~3 s or less is desirable [41]. When examining abdominal organs or tumors the

aorta is usually imaged, for thoracic imaging the ventricles of the heart or the pulmonary artery may be used, and for pelvic regions the iliac arteries may be employed; these vessels have cross-sectional areas that are large enough to allow AIFs to be extracted with minimal partial volume contamination. However, for other organs it can be a challenge to identify an adequate arterial supply and alternatives must be employed. For example, in the assessment of perfusion in breast lesions sometimes the left ventricle of the heart may be used, and in the brain the carotid may be employed, but both can suffer from problems with wash-in effects and coil sensitivity fall-off and, in the case of the carotid, substantial partial volume corruption. In such cases it may be necessary to use a surrogate for the AIF, such as the concentration time course in a draining vein (such as the sagittal sinus) or a population AIF. Alternatively, it may be possible to account for partial volume effects by using alternative AIF measurement strategies, such as dual bolus methods [42, 43], phase-based correction methods [44], or reference tissue methods [45]. Wash-in effects are reduced by ensuring that the blood is fully saturated (i.e., has experienced several ratio frequency [RF] pulses) by the time it reaches the location of the ROI [46].

The DCE sequence should ideally be run long enough to sample the enhancement plateau. If not, then v_e cannot be reliably measured, given that it only affects the plateau value, but not the rising portion of the curve (see Figure 4.3b). In tumors, this means that one must often scan for quite a long duration (up to 5–10 min).

An example of rapid DCE is shown in Figure 4.5. Imaging of the kidney and aorta at a temporal resolution of 2.5 s, using half the standard dose of Gd, allows the perfusion phase of the tissue signal to be seen, and it has a clear delay with respect to the aortic peak. In this organ the blood volume is large (about 30%), and can be estimated because the perfusion peak is so distinct. A modified Tofts' model fits the data well (Figure 4.4); in this model of the uptake phase (up to 90 s), the vascular delay and dispersion are accounted for, and there is no efflux from the parenchymal ROI. Renal filtration occurs mostly after bolus passage, and can be well estimated. Using this technique, GFR estimates in controls were in good agreement with normal literature values [26, 27, 47].

There is scope to optimize the FA when using spoiled gradient-echo acquisitions. A small FA gives more signal at low concentration, but has limited dynamic range (see Figure 4.6 FA = 5°); increasing the FA gives increased sensitivity to Gd (Figure 4.6 FA = 10°); further increases (Figure 4.6 FA = 20° or 30°) give a wider dynamic range (at the expense of reduced sensitivity) and are needed if measuring the AIF (peak blood concentration 6 mM [16], see Figure 4.7) together with tissue enhancement. Non-linear dependence of signal on Gd concentration is not a concern as it is properly dealt with in the MRI model. However, large changes in T_2^* during the initial stages after contrast agent administration may affect the measurement when using spoiled gradient echo methods. This can be minimized by using the shortest possible TE.

Motion artifacts

Breathing can cause serious artifacts in body imaging, particularly in locations close to the diaphragm. Some data suggest this may only be a small effect and may not contribute to overall measurement reproducibility [40]. However, we suggest some potential approaches to minimizing its effect:

1. Allow free breathing. Some centers minimize diaphragm movement by having one or both hands above the head. Any residual motion can be compensated for using image registration in post-processing, although the changing contrast observed during the DCE-MRI time course means that specially tailored registration methods may be required [40].
2. Breath-hold for first pass (~20 s) then allow breathing (although this can result in a large movement as breathing resumes). Also the position of the abdominal tissues during breath-hold may be different to all the other points in the time series, necessitating image registration. Some patients may also find it difficult to maintain a good breath-hold for 20 s.
3. Free breathe and discard data at the extremes of position (using the images, navigator gating or respiratory monitoring to detect the extrema) or apply image registration. However, discarding images can lead to important time points during the DCE-MRI and AIF series being missed, which is particularly critical during the first pass of contrast agent.
4. Guided free breathing (instructions from the imaging technologist).

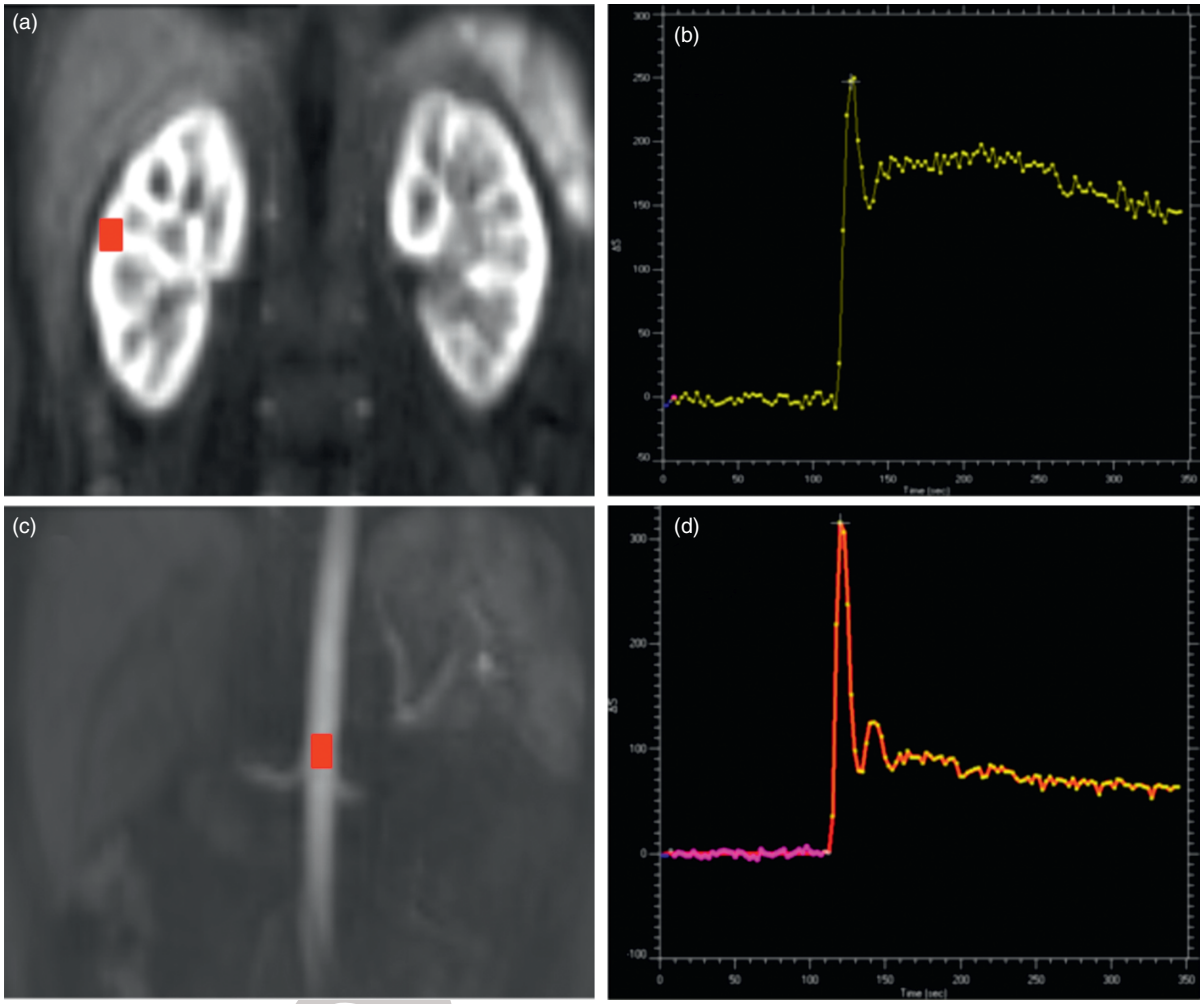

Figure 4.5 Signal enhancement in kidney and aorta. A cortical ROI (a) is used to define the time of peak enhancement (b), and the arterial ROI (c) gives the blood curve (d).

Whether breathing should be controlled or not is currently unclear (this may depend on the kind of patient, and the availability of registration – see below), and is the subject of ongoing research.

Flip angle accuracy

FA accuracy is often poor, but is crucial if tissue parameters such as K^{trans} are to be determined accurately. It affects the calculation of concentration from enhancement (Eq. (4.3)), the estimation of the AIF, and the measurement of T_{10}. B_1 non-uniformity (heterogeneity), if present, means that the FA distribution is also non-uniform. There are two primary causes of such non-uniformity. First, dielectric resonance produces standing waves in the subject, which are more pronounced at higher fields (e.g., 3 T) and in larger objects (the effect is greater in the body than in the head and can be significant even at 1.5 T [48]). Second, smaller transmit coils are less uniform, and therefore the body transmit coil is to be preferred (not a smaller combined transmit/receive coil). During the FA setup procedure, a good technique, if available, will optimize the FA over just the volume to be imaged (not the whole slice), and an accurate FA may then be obtained in spite of more global FA non-uniformity. An additional source of FA error is in 2D multi-slice imaging, where the slice profile is often poor, leading to varying FA across the slice [49, 50]. Therefore 3D (volume) acquisitions are preferred.

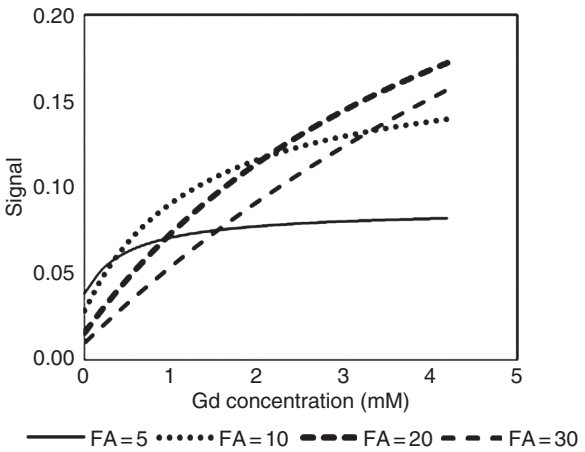

Figure 4.6 Signal intensity for a gradient echo sequence with various FA values. Eqs. (4.2) and (4.3) were used, with TR = 3 ms and $T_1 = 1$ s.

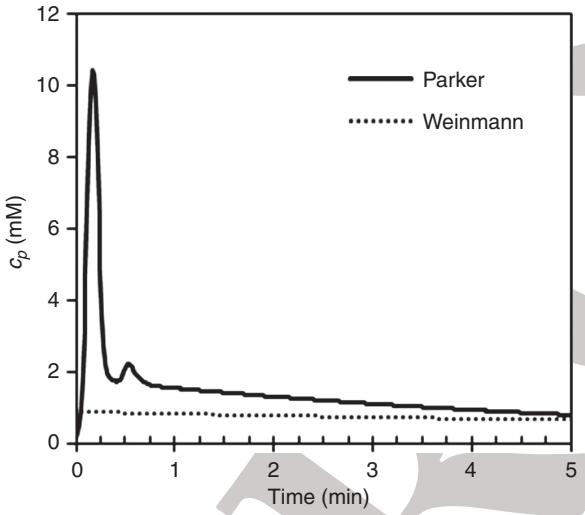

Figure 4.7 Population average AIFs (dose = 0.1 mmol/kg).

B_1 maps can be measured quite quickly [51] (< 2 min) and these may enable corrections to be made in the presence of FA inaccuracy and inhomogeneity. Transmit phased array technology is in development, which provides the ability to produce more homogeneous B_1 fields over the ROI within the subject, and these so-called "RF shimming" methods may enable acquisitions with more uniform and accurate FA values. Note that all manufacturers develop simple dual- or multiple-transmitter systems for their 3 T systems, and some of these systems are already available today.

The tissue T_1 value (T_{10}) can be measured, or else a standard value from the literature used. An accurate measurement is preferred for each individual subject, since in dis[illegible] this can alter; this can often be carried out i[illegible] 5 [illegible]. The most common method is the varia[illegible] method, where gradient echo sequences with several FA values are used. These include a mostly proton density-weighted sequence (low FA) and one or more T_1-weighted sequence (higher FA). Clearly the T_{10} accuracy is crucially dependent on the FA accuracy. Inversion recovery methods (with variable inversion time [TI], fixed FA) are more robust, but usually slower.

An error in the T_{10} value will in turn usually give an incorrect value for the tissue concentration (Eq. (4.1)). Thus if T_{10} has been measured badly, or if an incorrect standard value from the literature has been used, then gross errors in tissue parameters such as K^{trans} can ensue, particularly if literature values are used for a tissue which has a wide range of possible T_{10} values. An example from breast cancer shows that for a range of feasible T_{10} literature values used in the fitting process, the fits to a given image intensity dataset are equally good, K^{trans} can vary by at least a factor of 2, and v_e can reach impossible values ($v_e > 100\%$) [52]; see Table 4.1. k_{ep} is relatively robust (as long as the vascular volume [v_p] is negligible). An increase of 1% in T_{10} gives a resulting decrease of 1% in K^{trans}, such that the product remains approximately constant.

choice of contrast agent

Any contrast agent can in principle be used for DCE methodology, provided it is stable and transport is passive (i.e., there is no active transport mechanism which would be concentration-dependent or favor transport in one direction over the other – see Eq. (4.5)). The initial work [5] was carried out with Gd-DTPA (Magnevist, size 938 Da). Clearly larger molecules will have lower permeability and hence possibly lower K^{trans} values (Eqs. (4.7) and (4.8)). The AIF may alter a little with viscosity (increased viscosity could slow down the mixing of the bolus into the blood pool). Contrast agents with larger molecular weight potentially can separate out the effects of permeability and perfusion on uptake, although the compound must be stable, with a single form in the bloodstream, and imaging times become longer. In view of the concerns about nephrogenic

Table 4.1. Sensitivity of tissue parameters to assumed T_{10} value taken from the literature

Tissue	T_{10} (s)	K^{trans} (min^{-1})	v_e (%)	Residual in fit	k_{ep} (min^{-1})	K^{trans} T_{10}
Normal low-risk fatty portion	0.46	0.88	143	0.091	0.62	0.41
Tumor – low T_{10}	0.60	0.63	96	0.092	0.65	0.38
Normal high-risk diffuse density portion	0.71	0.51	76	0.093	0.67	0.36
Tumor – high T_{10}	1.3	0.26	36	0.095	0.72	0.34

Adapted from Tofts *et al.* [52]

systemic basis, there will be value in gaining experience using the newer cyclic compounds. In addition to Magnevist, potentially suitable candidate compounds (not all cyclic) are: Dotarem (754 Da), Eovist (725 Da), Gadovist (605 Da), Omniscan (574 Da), Optimark (662 Da), and ProHance (559 Da) (see http://www.rxlist.com). Different contrast media have different blood pool clearance rates, which may affect the AIF for DCE-MRI when long time series are being acquired. In particular, those agents that demonstrate clearance via the liver as well as the kidney (e.g., MultiHance [gadobentate dimeglumine] or Primovist/Eovist [gadoxetic acid disodium]) may demonstrate different blood kinetics to those that are cleared only via the kidneys. However, little research has been performed to date into the differences in AIFs that are likely to be observed when using different contrast media.

Image analysis

Analysis can be carried out on individual ROIs, or on a pixel-by-pixel basis to produce a map for the whole organ. The reduction of motion artifact using spatial registration, if available, is likely to improve the quality of the fit (depending on the tissue location). In-plane movement is relatively easy to remove, but because motion in the body is non-rigid, effective removal is much harder than in the brain, and a topic of ongoing research. Evidence suggests that while it is possible to correct for motion in DCE-MRI time series, the process of model fitting is relatively robust to periodic motion, meaning that quiet steady breathing may not introduce as many confounds as may be feared [40]. However, non-periodic motion (such as a bulk shift of the body) and very large breathing-related motion are likely to cause problems in the modeling output and should ideally be corrected.

The pharmacokinetic models described above require knowledge of the arterial plasma concentration $c_p(t)$; this is the arterial input function (AIF) calculated from the whole blood signal (which confusingly is sometimes called the "AIF," even though it contains both plasma and erythrocytes). It can be measured for each subject, and thus within- and between-subject variation can be taken into account, although if the technique is not implemented well, it can introduce extra variation which contaminates the final measurements of tissue physiology.

Alternatively, a population average AIF can be used. Some of these are described analytically (i.e., using mathematical equations, rather than just a list of numbers), which makes them more convenient to use. In particular they are available at any temporal resolution. The most popular are the original biexponential Weinmann plasma curve [15], derived from low temporal resolution arterial blood samples, and the more complex Parker blood function [16], derived from high temporal resolution MRI data. Horsfield's functional form [17] for the AIF needs a single measurement of absolute concentration. In the Parker function, bolus first pass and recirculation are represented. After bolus passage and recirculation, the MRI measurement for a standard dose of 0.1 mmol/kg (Parker $c_p[1\ \text{min}] = 1.53$ mM assuming Hct = 42%) is considerably higher than the direct measurement (Weinmann $c_p[1\ \text{min}] = 0.82$ mM); however, the estimates are within the error bars of the two experimental results, indicating that they are likely to be compatible. Possible reasons for residual discrepancy include a population difference (the Parker AIFs were drawn from a population of cancer patients and the Weinmann AIFs from healthy volunteers; in neither case was a measured Hct used) and wash-in effects in the MRI method. Although the Weinmann input function was derived from blood samples with a

temporal sampling too slow to capture the detail clearly present up to about 40 s (see Figure 4.7), by 1 min we expect the Weinmann values to be unaffected by this bolus mixing effect. The numerical AIFs of Fritz-Hansen *et al.* [53] showed excellent agreement between an inversion recovery MRI method and rapid direct blood measurements; their values (approximate mean over six subjects $c_p(1\ \text{min}) = 1.09$ mM; range 0.86–1.64 mM; assumed Hct = 0.42) are closer to the Weinmann value but overlap with the Parker value (mean over 67 DCE-MRI measurements $c_p(1\ \text{min}) = 1.8 \pm 0.5$ mM [SD]; assumed Hct = 0.42). The choice of AIF will depend on the tissue being studied and the sequences available.

When it comes to the modeling of the tissue signal, several versions can be considered. For "Tofts', modeling" the primary free parameters are K^{trans} and either k_{ep} or v_e (since k_{ep} and v_e are related). It is worth including v_p to see if the fit improves (but without inducing overfitting), and whether there is a systematic effect on the fitted K^{trans} and v_e values.

The onset time of the bolus *t_onset* should be included in the fitting process as there will be a variable delay between the location of AIF measurement and the tissue of interest. Similarly, onset time estimation will be needed if a population average AIF is used (since the timing of bolus arrival with respect to the start of tissue enhancement is unknown). The appropriate approach will again depend on the organ and the temporal resolution.

The mathematical process of fitting the model to the data works as follows. The model signal can be calculated for many combinations of the free parameters (K^{trans}, etc., Table 4.2). For each of these combinations, the differences between the model signal value (at each time point) and the measured data are found. These differences are squared and summed across each time point to provide a "total "difference." The free parameters are adjusted until this total difference is minimized. The model has then been "fitted" to the data. This is called the "least squares solution." The differences between the data and the

Table 4.2. Fixed and free parameters in DCE modeling

Quantity	Symbol	Units	Type
Perfusion (of blood)[a]	F	ml blood/min (100 ml tissue)$^{-1}$	Free
Flip angle[b]	FA	degrees	Fixed; may require B_1 mapping to provide accurate values
Hematocrit[c]	Hct	%	Fixed; measure independently if possible Approximate normal ranges: males 40–52%; females 36–48%. Textbook value is 41% [12]
Onset time	*t_onset*	s	Free
Rate constant[d]	k_{ep}	min^{-1}	Free
Transfer constant	K^{trans}	min^{-1}	Free
T_1 relaxivity	r_1	s^{-1} mM^{-1}	Fixed (4.5 s^{-1} mM^{-1}). May vary in vivo but currently not possible to measure
T_1 of blood	T_{10}^{blood}	s	Fixed (measured)
T_1 of tissue	T_{10}	s	Fixed (measured)
TR	TR	s	Fixed
Fractional volume of EES[e]	v_e	$0 < v_e < 100\%$	Free
Fractional volume of blood plasma in tissue	v_p	$0 < v_p < 100\%$	Free

[a] Plasma perfusion F_p is more reliably measured, and an unambiguous symbol for blood perfusion is F_b (see text)
[b] θ is the flip angle in degrees (used in Eq. (4.3))
[c] Small vessel hematocrit is considerably lower (see text)
[d] $k_{ep} = K^{\text{trans}}/v_e$
[e] Extravascular extracellular space

fitted model are called "residuals" (e.g., Figure 4.5). From these can be found the "root-mean-square residual," which is a kind of average difference between the model and the data, and which gives an indication of the quality of the model and of the fit. If the residuals appear random in character then these probably derive from a random effect such as image noise or movement; if there seems to be a systematic pattern to the residuals then the model can often be improved.

For any fitting procedure, basic tests should be carried to ensure that the procedure converges properly (i.e., that the fitted parameters are independent of the starting values), and reformulation of the free parameters to decrease their interdependence may be required. "Fit failures" can occur, particularly if the data are noisy (e.g., deriving from single pixels instead of an ROI); no valid parameter values are produced for that dataset. In the fitting process it is important to identify and flag these failures, so that the output (i.e., invalid parameter values) does not contaminate any subsequent analysis. Values of $v_e > 100\%$ may occur if an incorrect value of T_{10} has been used (see Table 4.1), if v_p has not been incorporated in the fit when needed, or if the enhancement peak has not been reached (see Figure 4.3b). It is also helpful to test to see if any detectable enhancement has occurred prior to fitting a model in order to avoid fitting to a signal that is indistinguishable from noise, as this can lead to randomly erroneous parameters. It has also been shown that quantification of the amount of tumor that does not enhance is in itself a useful parameter to extract from the DCE-MRI time series [54–56]. Note that recent developments in the field allow for nested modeling of both "Tofts models", with or without v_p, with automatic selection of one model over the next one based on an F test [57].

Fitting can be implemented in three ways. The simplest and most straightforward way is to use ROI data (which are inherently low noise) and put these into a spreadsheet (e.g., Microsoft Excel running on a PC). The mathematics can be set up using inbuilt formula functions, and the "solver" function can carry out the minimization process. The more complex way is to set up pixel-by-pixel mapping, either using a standard environment (e.g., Matlab) or by obtaining this from a supplier. Pixel mapping is more likely to benefit from spatial registration of the images to reduce the effect of motion; the operation is much more computer-intensive, and the single-pixel data are inherently noisy, so care must be taken to identify fit failures. The benefits of pixel mapping include the abilities to interrogate all the tissue without bias, and to generate histograms and other measures of tissue or tumor heterogeneity, which have potential utility [58, 59]. The third possibility is to use commercially available software, which is currently available from third parties and also from at least one mainstream MRI vendor.

Histograms can show the distribution of parameter values, in a region or volume of interest. By taking care of histogram generation and architecture,

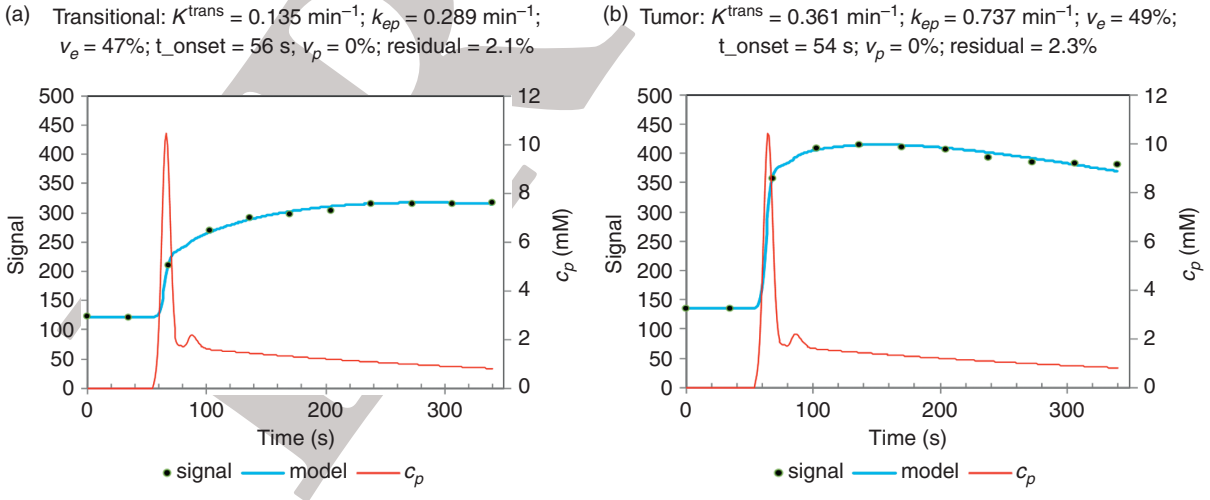

Figure 4.8 Modeling of prostate cancer DCE data. The Parker AIF was used (Figure 4.7), with $v_p = 0$. Although data were only acquired every 34 s, the model was calculated with a temporal resolution of 1 s. Spreadsheet output is shown for (a) transitional tissue and (b) tumor ROIs (data from University of Miami).

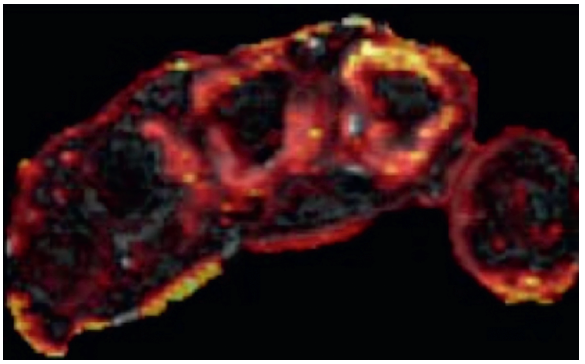

Figure 4.9 A K^{trans} map showing the joints of the hand of a patient suffering from rheumatoid arthritis. The presence of inflammation in the joints leads to additional blood vessel recruitment and leaky vasculature, making DCE-MRI a potentially useful way to monitor disease and therapeutic intervention [64].

histograms become more useful and comparisons are more easily made [60]. The y-values can be calculated such that the area under the histogram curve is either the total volume under interrogation (in ml), or 100% (i.e., the histograms are normalized). Features such as peak location and height can be extracted from histograms. Characterizing the distribution tails can have predictive value [55] [61], and principle component analysis of the histogram shape can be powerful [62].

An example of using a spreadsheet to implement modeling of ROI data is shown in Figure 4.8. The prostate data have quite low temporal resolution (34 s), T_{10} had to be assumed (1.5 s), and a Parker AIF was used. Including the v_p term did not improve the fitting (and in fact it became rather unstable), probably because prostate perfusion is low [63] and

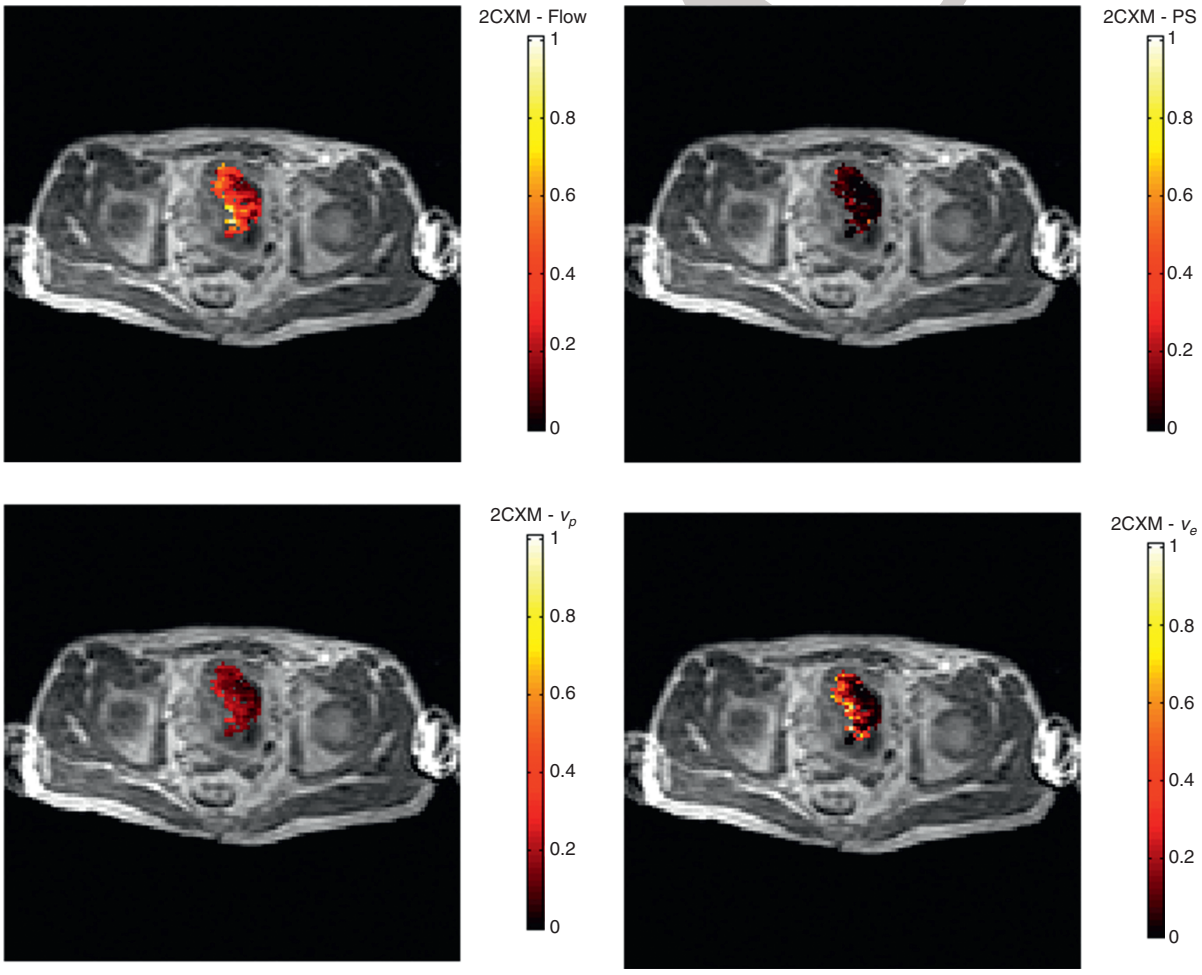

Figure 4.10 An example of the application of the 2CXM model in a patient with prostate cancer, providing measures of flow, PS, v_p, and v_e.

the temporal resolution coarse. In several ROIs from the same subject, fitted onset time agreed within 2 s, suggesting that it can be found quite reliably.

Examples of parametric maps based on pixel-by-pixel analysis are shown in Figures 4.9 and 4.10; Figure 4.9 shows a K^{trans} map from the hand of a patient with rheumatoid arthritis, while Figure 4.10 shows various permeability and flow parameters derived from the 2CXM model in a patient with prostate cancer.

Conclusions

The principle physiological parameters that can be measured with DCE-MRI are the transfer coefficient K^{trans} (related to capillary permeability, surface area and perfusion) and v_e the size of the EES, although additional useful parameters are measurable given appropriate sequences and analysis methods. To do this needs good control of FA and an accurate measurement of tissue T_1 before injection of Gd. If T_1 measurement is not available, then it may be possible to use a standard value; in any case the rate constant k_{ep} can still be measured, which is probably useful. The possible and optimum acquisition protocols and models will depend on which tissue is being imaged.

Acknowledgments

David Collins and Martin Leach (both Institute of Cancer Research, UK), and David Buckley (University of Leeds, UK) contributed valuable insight into DCE imaging. Isky Gordon (University College London, UK) and Iosif Mendichovszky (University of Manchester, UK) provided data for Figure 4.5. Peter Gall (Siemens medical) contributed the list of CA's. Radka Stoyanova (University of Miami, USA) provided data for Figure 4.9. Penny Hubbard (University of Manchester, UK) provided Figure 4.10.

Appendix

Model parameters

There are several kinds of parameters used in the model. *Fixed* parameters (*FA, TR, Hct,* T_{10}, T_{10}^{blood}, r_1) have preset values which are required before fitting can start. *Free* parameters (K^{trans}, v_e, k_{ep}, and maybe v_p and t_onset) are varied and then estimated as part of the fitting process. Other parameters (c_p, etc.) are used temporarily as part of the process of modeling the signal. The fixed and free parameters are summarized in Table 4.2.

References

1. Jackson A, Buckley DL, Parker GJ. *Dynamic Contrast-Enhanced Magnetic Resonance Imaging in Oncology*. Berlin: Springer, 2004.
2. Tofts PS.*Quantitative MRI of the Brain: Measuring Changes Caused by Disease*. New York: Wiley, 2003.
3. Tofts PS, Brix G, Buckley DL, *et al.* Estimating kinetic parameters from dynamic contrast-enhanced T(1)-weighted MRI of a diffusable tracer: standardized quantities and symbols. *J Magn Reson Imaging* 1999;**10**:223–32.
4. Leach MO, Brindle KM, Evelhoch JL, *et al.* The assessment of antiangiogenic and antivascular therapies in early-stage clinical trials using magnetic resonance imaging: issues and recommendations. *Br J Cancer* 2005;**92**:1599–610.
5. Tofts PS, Kermode AG. Measurement of the blood-brain barrier permeability and leakage space using dynamic MR imaging. 1. Fundamental concepts. *Magn Reson Med* 1991;**17**:357–67.
6. Naish JH, McGrath DM, Bains LJ, *et al.* Comparison of dynamic contrast-enhanced MRI and dynamic contrast-enhanced CT biomarkers in bladder cancer. *Magn Reson Med* 2011; **66**: 219–26.
7. Yang C, Stadler WM, Karczmar GS, *et al.* Comparison of quantitative parameters in cervix cancer measured by dynamic contrast-enhanced MRI and CT. *Magn Reson Med* 2010;**63**: 1601–9.
8. Tofts PS, Shuter B, Pope JM.Ni-DTPA doped agarose gel–a phantom material for Gd-DTPA enhancement measurements. *Magn Reson Imaging* 1993; **11**:125–33.
9. Shuter B, Tofts PS, Wang SC, Pope JM.The relaxivity of Gd-EOB-DTPA and Gd-DTPA in liver and kidney of the Wistar rat. *Magn Reson Imaging* 1996;**14**:243–53.
10. Stanisz GJ, Henkelman RM. Gd-DTPA relaxivity depends on macromolecular content. *Magn Reson Med* 2000;**44**:665–7.
11. Spees WM, Yablonskiy DA, Oswood MC, Ackerman JJ. Water proton MR properties of human blood at 1.5 Tesla: magnetic susceptibility, T(1), T(2), T*(2), and non-Lorentzian signal behavior. *Magn Reson Med* 2001;**45**:533–42.
12. Boron WF, Boulpaep EL. *Medical Physiology*. Philadelphia: Saunders, 2008.
13. Roberts C, Hughes S, Naish JH, *et al.* Individually Measured

Hematocrit in DCE-MRI studies. *Proceedings of the International Society for Magnetic Resonance in Medicine*, Montreal, Canada, 2011; 1078.

14. Kety SS. The theory and applications of the exchange of inert gas at the lungs and tissues. *Pharmacol Rev* 1951;**3**:1–41.
15. Weinmann HJ, Laniado M, Mutzel W. Pharmacokinetics of GdDTPA/dimeglumine after intravenous injection into healthy volunteers. *Physiol Chem Phys Med NMR* 1984;**16**:167–72.
16. Parker GJ, Roberts C, Macdonald A, *et al.* Experimentally-derived functional form for a population-averaged high-temporal-resolution arterial input function for dynamic contrast-enhanced MRI. *Magn Reson Med* 2006;**56**:993–1000.
17. Horsfield MA, Thornton JS, Gill A, *et al.* A functional form for injected MRI Gd-chelate contrast agent concentration incorporating recirculation, extravasation and excretion. *Phys Med Biol* 2009;**54**:2933–49.
18. Tofts PS.Modeling tracer kinetics in dynamic Gd-DTPA MR imaging. *J Magn Reson Imaging* 1997;**7**:91–101.
19. Sourbron SP, Buckley DL. On the scope and interpretation of the Tofts models for DCE-MRI. *Magn Reson Med* 2011;**66**:735–45.
20. Sourbron SP, Buckley DL. Tracer kinetic modelling in MRI: estimating perfusion and capillary permeability. *Phys Med Biol* 2012; **57**:R1–33.
21. Pries AR, Ley K, Gaehtgens P. Generalization of the Fahraeus principle for microvessel networks. *Am J Physiol* 1986;**251**:H1324–32.
22. Crystal GJ, Downey HF, Bashour FA. Small vessel and total coronary blood volume during intracoronary adenosine. *Am J Physiol* 1981;**241**:H194–201.
23. Sakai F, Nakazawa K, Tazaki Y, *et al.* Regional cerebral blood volume and hematocrit measured in normal human volunteers by single-photon emission computed tomography. *J Cereb Blood Flow Metab* 1985;**5**:207–13.
24. Rempp KA, Brix G, Wenz F, *et al.* Quantification of regional cerebral blood flow and volume with dynamic susceptibility contrast-enhanced MR imaging. *Radiology* 1994;**193**:637–41.
25. Gaehtgens P.Flow of blood through narrow capillaries: rheological mechanisms determining capillary hematocrit and apparent viscosity. *Biorheology* 1980;**17**:183–9.
26. Tofts PS, Cutajar M, Mendichovszky IA, Gordon I. Accurate and precise measurement of renal filtration and vascular parameters using DCE-MRI and a 3-compartment model. *Proceedings of the International Society for Magnetic Resonance in Medicine*, Stockholm, Sweden, 2010; 326.
27. Tofts PS, Cutajar M, Mendichovszky IA, Peters AM, Gordon I.Precise measurement of renal filtration and vascular parameters using a two-compartment model for dynamic contrast-enhanced MRI of the kidney gives realistic normal values. *Eur Radiol* 2012;**22**: 1320–30.
28. St Lawrence KS, Lee TY. An adiabatic approximation to the tissue homogeneity model for water exchange in the brain: I. Theoretical derivation. *J Cereb Blood Flow Metab* 1998;**18**:1365–77.
29. Donaldson SB, West CM, Davidson SE, *et al.* A comparison of tracer kinetic models for T1-weighted dynamic contrast-enhanced MRI: application in carcinoma of the cervix. *Magn Reson Med* 2010;**63**:691–700.
30. Hatabu H, Tadamura E, Levin DL, *et al.* Quantitative assessment of pulmonary perfusion with dynamic contrast-enhanced MRI. *Magn Reson Med* 1999;**42**:1033–8.
31. Ohno Y, Hatabu H, Murase K, *et al.* Quantitative assessment of regional pulmonary perfusion in the entire lung using three-dimensional ultrafast dynamic contrast-enhanced magnetic resonance imaging: preliminary experience in 40 subjects. *J Magn Reson Imaging* 2004;**20**:353–65.
32. Jerosch-Herold M. Quantification of myocardial perfusion by cardiovascular magnetic resonance. *J Cardiovasc Magn Reson* 2010;**12**:57.
33. Naish JH, Kershaw LE, Buckley DL, *et al.* Modeling of contrast agent kinetics in the lung using T1-weighted dynamic contrast-enhanced MRI.*Magn Reson Med* 2009;**61**:1507–14.
34. Brix G, Kiessling F, Lucht R, *et al.* Microcirculation and microvasculature in breast tumors: pharmacokinetic analysis of dynamic MR image series. *Magn Reson Med* 2004;**52**:420–9.
35. Sourbron S, Ingrisch M, Siefert A, Reiser M, Herrmann K. Quantification of cerebral blood flow, cerebral blood volume, and blood-brain-barrier leakage with DCE-MRI. *Magn Reson Med* 2009;**62**:205–17.
36. Brix G, Zwick S, Kiessling F, Griebel J. Pharmacokinetic analysis of tissue microcirculation using nested models: multimodel inference and parameter identifiability. *Med Phys* 2009;**36**:2923–33.
37. Johnson JA, Wilson TA. A model for capillary exchange. *Am J Physiol* 1966;**210**:1299–303.
38. Koh TS, Zeman V, Darko J, *et al.* The inclusion of capillary distribution in the adiabatic tissue homogeneity model of blood flow. *Phys Med Biol* 2001;**46**:1519–38.
39. Tofts PS. QA: quality assurance, accuracy, precision and phantoms. In: Tofts P, editor, *Quantitative MRI of the Brain: Measuring Changes Caused by Disease*. Chichester: John Wiley, 2003: 55–81.

40. Buonaccorsi GA, O'Connor JP, Caunce A, *et al.* Tracer kinetic model-driven registration for dynamic contrast-enhanced MRI time-series data. *Magn Reson Med* 2007;**58**:1010–19.

41. Henderson E, Rutt BK, Lee TY. Temporal sampling requirements for the tracer kinetics modeling of breast disease. *Magn Reson Imaging* 1998;**16**:1057–73.

42. Kostler H, Ritter C, Lipp M, *et al.* Prebolus quantitative MR heart perfusion imaging. *Magn Reson Med* 2004;**52**:296–9.

43. Risse F, Semmler W, Kauczor HU, Fink C. Dual-bolus approach to quantitative measurement of pulmonary perfusion by contrast-enhanced MRI. *J Magn Reson Imaging* 2006;**24**:1284–90.

44. Korporaal JG, van den Berg CA, van Osch MJ, *et al.* Phase-based arterial input function measurements in the femoral arteries for quantification of dynamic contrast-enhanced (DCE) MRI and comparison with DCE-CT.*Magn Reson Med* 2011; **66**:1267–74.

45. Yankeelov TE, Luci JJ, Lepage M, *et al.* Quantitative pharmacokinetic analysis of DCE-MRI data without an arterial input function: a reference region model. *Magn Reson Imaging* 2005;**23**:519–29.

46. Roberts C, Little R, Watson Y, *et al.* The effect of blood inflow and B(1)-field inhomogeneity on measurement of the arterial input function in axial 3D spoiled gradient echo dynamic contrast-enhanced MRI. *Magn Reson Med* 2011;**65**:108–19.

47. Buckley DL, Shurrab AE, Cheung CM, *et al.* Measurement of single kidney function using dynamic contrast-enhanced MRI: comparison of two models in human subjects. *J Magn Reson Imaging* 2006;**24**:1117–23.

48. Barker GJ, Simmons A, Arridge SR, Tofts PS. A simple method for investigating the effects of non-uniformity of radiofrequency transmission and radiofrequency reception in MRI. *Br J Radiol* 1998;**71**:59–67.

49. Brookes JA, Redpath TW, Gilbert FJ, Murray AD, Staff RT. Accuracy of T1 measurement in dynamic contrast-enhanced breast MRI using two- and three-dimensional variable flip angle fast low-angle shot. *J Magn Reson Imaging* 1999;**9**:163–71.

50. Parker GJ, Barker GJ, Tofts PS. Accurate multislice gradient echo T(1) measurement in the presence of non-ideal RF pulse shape and RF field nonuniformity. *Magn Reson Med* 2001;**45**:838–45.

51. Dowell NG, Tofts PS. Fast, accurate, and precise mapping of the RF field in vivo using the 180 degrees signal null. *Magn Reson Med* 2007;**58**:622–30.

52. Tofts PS, Berkowitz B, Schnall MD. Quantitative analysis of dynamic Gd-DTPA enhancement in breast tumors using a permeability model. *Magn Reson Med* 1995;**33**:564–8.

53. Fritz-Hansen T, Rostrup E, Larsson HB, Sondergaard L, Ring P, Henriksen O. Measurement of the arterial concentration of Gd-DTPA using MRI: a step toward quantitative perfusion imaging. *Magn Reson Med* 1996;**36**:225–31.

54. O'Connor JP, Jayson GC, Jackson A, *et al.* Enhancing fraction predicts clinical outcome following first-line chemotherapy in patients with epithelial ovarian carcinoma. *Clin Cancer Res* 2007;**13**:6130–5.

55. Donaldson SB, Buckley DL, O'Connor JP, *et al.* Enhancing fraction measured using dynamic contrast-enhanced MRI predicts disease-free survival in patients with carcinoma of the cervix. *Br J Cancer* 2010;**102**:23–6.

56. Mills SJ, Soh C, O'Connor JP, *et al.* Tumour enhancing fraction (EnF) in glioma: relationship to tumour grade. *Eur Radiol* 2009;**19**:1489–98.

57. Bagher-Ebadian H, Jain R, Nejad-Davarani SP, *et al.* Model selection for DCE-T1 studies in glioblastoma. *Magn Reson Med* 2011;**68**:241–51.

58. Rose CJ, Mills SJ, O'Connor JP, *et al.* Quantifying spatial heterogeneity in dynamic contrast-enhanced MRI parameter maps. *Magn Reson Med* 2009;**62**:488–99.

59. Canuto HC, McLachlan C, Kettunen MI, *et al.* Characterization of image heterogeneity using 2D Minkowski functionals increases the sensitivity of detection of a targeted MRI contrast agent. *Magn Reson Med* 2009;**61**:1218–24.

60. Tofts PS, Davies GR, Dehmeshki J. Histograms: measuring subtle diffuse disease. In: Tofts P, editor. *Quantitative MRI of the Brain: Measuring Changes Caused by Disease*. Chichester: John Wiley, 2003: 581–610.

61. Tofts PS, Benton CE, Weil RS, *et al.* Quantitative analysis of whole-tumor Gd enhancement histograms predicts malignant transformation in low-grade gliomas. *J Magn Reson Imaging* 2007;**25**:208–14.

62. Dehmeshki J, Ruto AC, Arridge S, *et al.* Analysis of MTR histograms in multiple sclerosis using principal components and multiple discriminant analysis. *Magn Reson Med* 2001;**46**:600–9.

63. Buckley DL, Roberts C, Parker GJ, Logue JP, Hutchinson CE.Prostate cancer: evaluation of vascular characteristics with dynamic contrast-enhanced T1-weighted MR imaging–initial experience. *Radiology* 2004;**233**:709–15.

64. Hodgson RJ, Barnes T, Connolly S, *et al.* Changes underlying the dynamic contrast-enhanced MRI response to treatment in rheumatoid arthritis. *Skeletal Radiol* 2008;**37**:201–7.